SCExAO: the first high contrast exoplanet imager on an ELT?

Julien Lozi[a], Nemanja Jovanovic[a], Olivier Guyon[a,b,c], Jared Males[b], Garima Singh[c], Danielle Doughty[a,b], Prashant Pathak[a,d], Sean Goebel[a,e], Tomoyuki Kudo[a], and Frantz Martinache[f]

[a]NAOJ - Subaru Telescope, 650 N A'ohoku Pl, Hilo, HI 96720, USA
[b]University of Arizona - Steward Observatory, 933 N Cherry Ave, Tucson, AZ 85719, USA
[c]NASA - JPL, 4800 Oak Grove Dr, Pasadena, CA 91109, USA
[d]Sokendai University, 1560-35 Kamiyamaguchi, Hayama, 240-0115, Japan
[e]University of Hawaii - Institute for Astronomy, 640 N Aohoku Pl #209, Hilo, HI 96720, USA
[f]Observatoire de la Côte d'Azur, Boulevard de l'Observatoire, 06300 Nice, France

ABSTRACT

The Subaru Coronagraphic Extreme Adaptive Optics (SCExAO) instrument, currently under development for the Subaru Telescope, optimally combines state-of-the-art technologies to study exoplanets and stellar environments at the diffraction limit, both in visible and infrared light (0.6 to 2.4 μm). The instrument already includes an ultra-fast visible pyramid wavefront sensor operating at 3.5 kHz, a 2k-actuator deformable mirror, a set of optimal coronagraphs that can work as close as 1 l/D, a low-order wavefront sensor, a high-speed speckle control loop, and two visible interferometric modules, VAMPIRES and FIRST. After the integration of the integral field spectrograph CHARIS and a Microwave Kinetic Inductance Detector (MKID) in 2016, SCExAO will be one of the most powerful and effective tools for characterizing exoplanets and disks. None of the ELTs include a high-contrast imager and spectrograph among the first generation of instruments. To address this, we propose to upgrade SCExAO and deliver it as a first light visitor instrument to the Thirty Meter Telescope (TMT), a decade before the second generation instruments come online. SCExAO's flexibility assures that it will include the latest technologies when it arrives on TMT, achieving the ultimate goal of characterizing the first terrestrial planets in the habitable zones of M-type stars.

Keywords: Extreme Adaptive Optics, Phase Mask Coronagraph, Low-Order Wavefront Sensor, Speckle Control, Visible Interferometer, MKID

1. INTRODUCTION

The Subaru Coronagraphic Extreme Adaptive Optics (SCExAO) instrument[1] is a high contrast imager installed on the Subaru telescope, behind the facility adaptive optics (AO) AO188.[2] It is optimized for very small Inner Working Angles (IWA), 1 to 3 λ/D. Unlike other high contrast instruments like the Gemini Planet Imager (GPI)[3] and Spectro-Polarimetric High-contrast Exoplanet REsearch (SPHERE),[4] SCExAO is constantly evolving to integrate the latest technologies, new concepts and more efficient detectors. This advantage makes SCExAO the prime high contrast instrument on an 8-meter class telescope before the Extremely Large Telescopes (ELTs) come online. It is also the best prototype to test the technologies required for the spectroscopic characterization of habitable rocky planets around M-type stars. Our ultimate goal is to prepare the instrument to become the first high contrast imager on an ELT, as a visitor instrument when the Thirty Meter Telescope (TMT)[5] is completed. By employing this approach of embracing advanced technologies, SCExAO will travel towards TMT and position itself as an extremely capable and competitive first generation visitor instruments. Along the way it will commission high-angular resolution imagers, an Integral Field Spectrograph (IFS)[6] and a Microwave Kinetic Inductance Detector (MKID),[7] which will enable advanced wavefront control in the focal plane.

Further author information: (Send correspondence to J.L. or N.J.)
J.L.: E-mail: lozi@naoj.org, Telephone: 1 808 934 5949
N.J.: E-mail: nem@naoj.org, Telephone: 1 808 934 5959

This paper presents the current state of SCExAO at Subaru, the readiness of its different modules, and how we will be able to characterize Earth-like planets in the Habitable Zone (HZ) of M-type stars on TMT.

2. OVERVIEW OF SCExAO

2.1 High Contrast Imaging

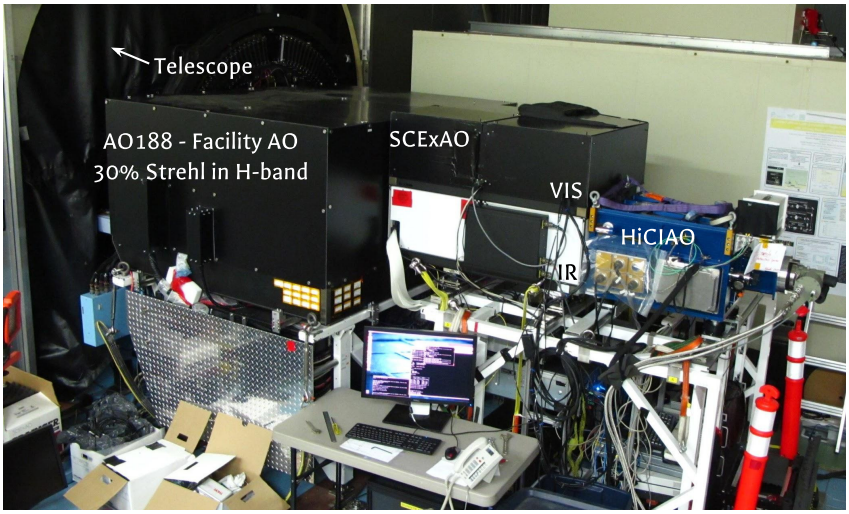

Figure 1. SCExAO bench on the Nasmyth platform of the Subaru Telescope. SCExAO is between the facility instrument AO188 and the IR camera HiCIAO.

The heart of the SCExAO instrument is its Extreme AO (ExAO) loop. But all the wavefront correction is not done inside the instrument. SCExAO is placed behind AO188 (see Fig. 1 to take advantage of a first stage of wavefront correction. Indeed, AO188 provides a Point Spread Function (PSF) with a Strehl ratio of about 30% in H-band.[2]

The high-contrast imaging capability of SCExAO is achieved in four steps:

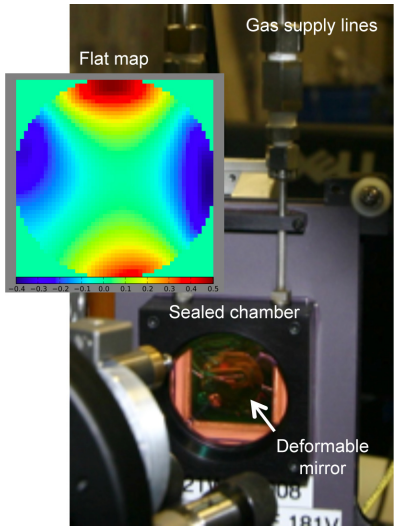

Figure 2. Picture of the 2000-actuator BMC deformable mirror used for high-contrast imaging. The map presented here is the map used to flatten the DM.

1. Extreme AO with a fast diffraction limited wavefront sensor: A visible Pyramid Wavefront Sensor (PyWFS, 700–900 nm),[8] corrects the residual wavefront at up to 3.5 kHz, using a 2000-actuator Deformable Mirror (DM, see Fig. 2), for spatial frequencies up to 22.5 λ/D.

2. Fast near infrared (NIR) speckle control:[9] Using a fast photon counting detector in NIR, a speckle control loop modulates, calibrates and removes residual speckles on one half of the image plane, down to $\sim$2 λ/D. Since SCExAO has only one DM, the control is implemented by sending offsets to the PyWFS control loop.

3. Small IWA and high throughput phase mask coronagraphs: A large choice of highly efficient coronagraphs —vector vortex,[10] 8-octant phase mask (8OPM),[11] Phase-Induced Amplitude Apodization (PIAA) coronagraphs[12]— can be used in order to cancel most of the starlight reaching the science detector.

4. NIR Lyot-based Low-Order Wavefront Sensor (LLOWFS):[13] If a coronagraph is used, low-order aberrations upstream of the phase mask can be measured using the rejected starlight. Using a fast NIR detector, a control loop is implemented to correct a few dozen Zernike modes, sending once again offsets to the PyWFS control loop.

2.2 SCExAO's Modules

As presented in Fig. 3, the SCExAO instrument is composed of different modules distributed on two main benches, and two side benches. The bottom bench is analyzing the IR part of the spectrum —y, J, H and K bands. The light coming from AO188 is collimated to image the pupil on the 2k-actuator DM. A dichroic then separates visible and IR light (cutoff at 940 nm). The visible light is sent to the top bench using a periscope, while the IR light is transmitted to the rest of the bench. PIAA optics can be inserted to perform a lossless apodization of the beam,[14] for coronagraphs or optimal injection into a single mode fiber,[15] for high resolution spectroscopy. The beam is then focused onto a coronagraphic phase mask, to reject the starlight outside of the pupil. A Lyot mask placed in the pupil plane removes that starlight, transmitting most of the light coming from a potential companion, or circumstellar disk, and some residual starlight. The Lyot mask is actually reflective outside the boundaries of the pupil, sending the rejected starlight toward the LLOWFS camera. The light unblocked by the Lyot stop is sent towards different science detectors:

1. A fast 170-Hz NIR detector, used mainly for alignment and characterization of the bench.

2. SAPHIRA,[16] a fast 1-kHz photon-counting detector in H-band, developed by the Institute for Astronomy (IfA) in Hilo, Hawaii, and used for fast speckle calibration and ultimately speckle nulling.

3. CHARIS,[6] an IFS developed by Princeton University, which will be commissioned mid-2016. It will provide high-resolution spectra in J, H or K band, or low-resolution spectra in these three bands simultaneously.

4. MKID Exoplanet Camera (MEC),[7] developed by University of California Santa Barbara, which is a photon-counting energy-discriminating camera, and planned to be commissioned early 2017. This new technology will allow SCExAO to achieve a better speckle characterization, using the wavelength information. This new technology is essential to achieve the necessary contrast to characterize Earth-like planets with TMT.

On the top bench, the visible light is decomposed into several bandwidths for several modules:

1. The PyWFS (800–900 nm): The light is focused on a pyramid shaped optics, and eventually modulated around the apex of this pyramid using a fast tip/tilt mirror, to separate the light into 4 pupils, imaged on a fast EMCCD detector, the First Light Imaging OCAM2k.

2. The Visible Aperture Masking Polarimetric Interferometer for Resolving Exoplanetary Signatures (VAMPIRES, 600–800 nm):[17] Using aperture masks and a fine measurement and calibration of the polarization, VAMPIRES can detect faint structures at a few mas of the star, like dust shells around post-AGB stars, or protoplanetary disks.

3. The Fibered Imager for a Single Telescope (FIRST, 600–800 nm):[18] The pupil is decomposed in segments that are injected into single mode fibers, reordered in a non-redundant linear pattern, recombined and spectrally decomposed onto an EMCCD camera. FIRST can detect very close companions (stars, giant planets) at a few mas of the main star.

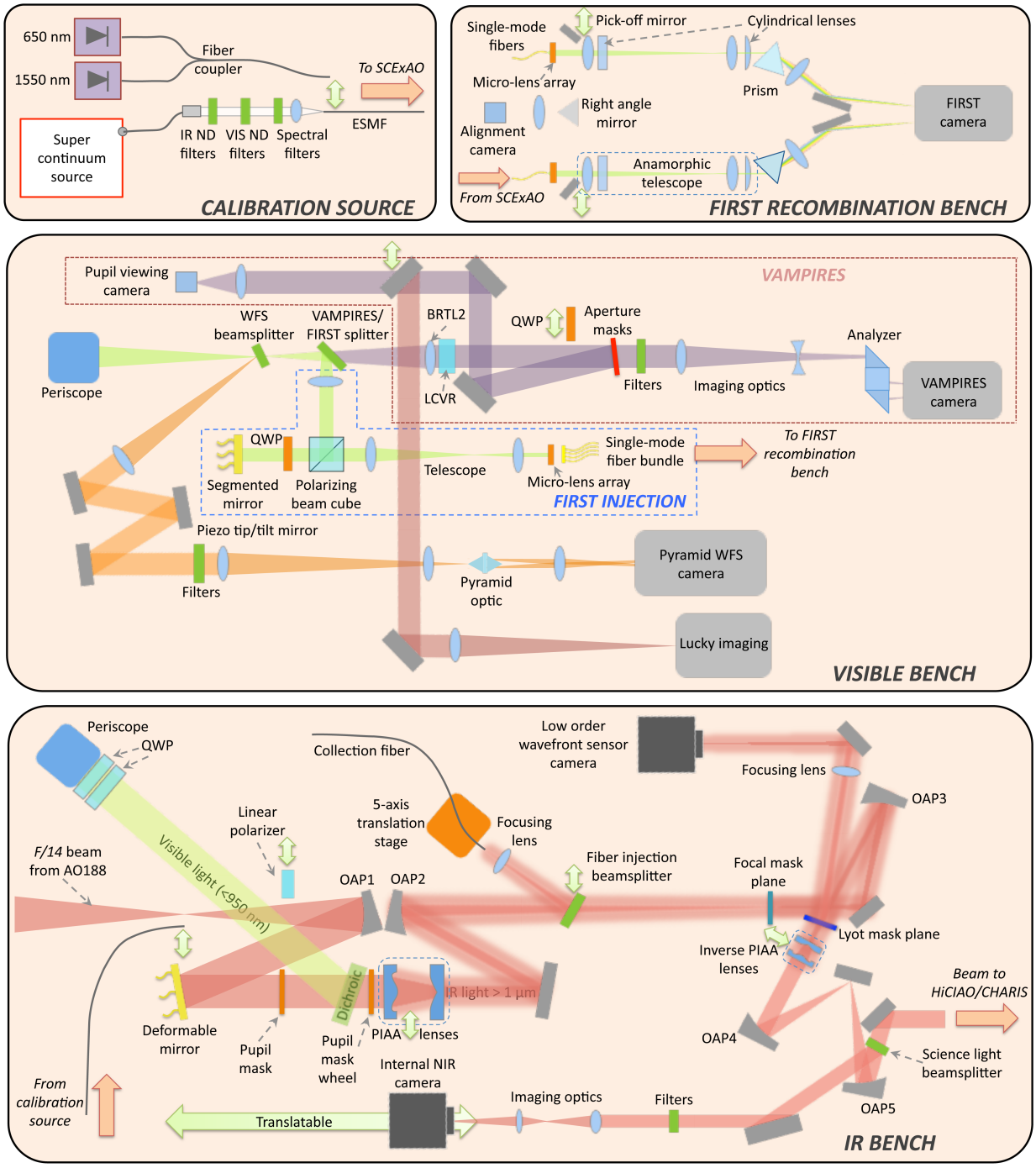

Figure 3. Schematic of the optical path inside the SCExAO instrument, dispersed on 4 benches.

3. WAVEFRONT CONTROL LOOPS

3.1 Performances Of The Pyramid Wavefront Sensor

The hardware implementation of the PyWFS is presented in Fig. 4. The pupil of the telescope is reimaged on the fast tip/tilt mirror on the right, to perform a modulation of the PSF around the apex of the pyramid shaped optics. Before that, a filter wheel allows us to select the central wavelength and bandwidth of the light used for

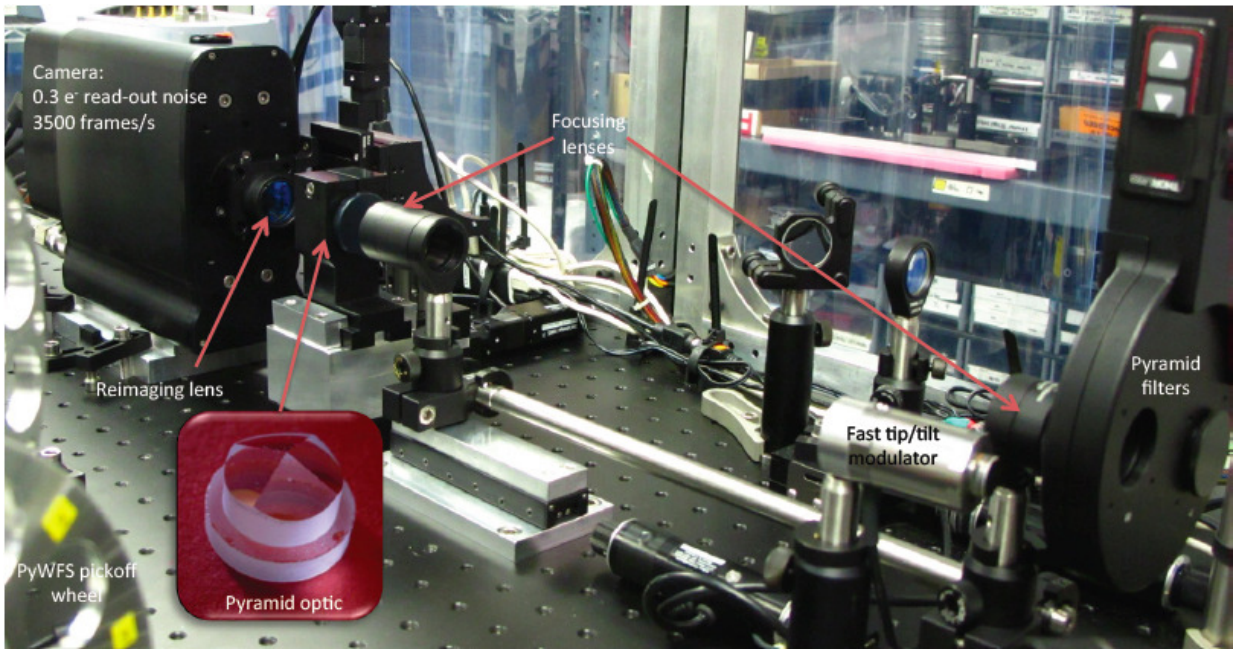

Figure 4. Hardware of the pyramid wavefront sensor on SCExAO. The pyramid optics is borrowed from MagAO, and the camera is a First Light Imaging OCAM2k.

wavefront sensing. A double lens system focuses the beam on the pyramid optics, borrowed from the Magellan Adaptive Optics (MagAO).[19] The beam is then separated in four parts, and a reimaging lens images four adjacent pupils on the detector. The camera used for wavefront sensing is the First Light Imaging OCAM2k, a visible EMCCD with 0.3 e^- readout noise, and a maximum frame rate of 3.5 kHz in binning mode (120×120 pixels).

The DM used for the wavefront correction is the 2k-actuator DM from Boston Micromachines (see Fig. 2), that has 50 actuators in the diameter. The pupil imaged on this DM is a bit smaller, with 45 actuators in the diameter, which allows us to correct spatial frequencies up to 22.5 λ/D. With the central obstruction and the spiders, only 1600 actuators are illuminated and driven by the loop. To avoid any effects on the edges of the pupil, the actuators that are partially illuminated are enslaved to neighboring actuators, which mean that the PyWFS loop only controls 1200 orthogonal modes.

Using a bank of 5 Graphics Processing Units (GPUs), the calculation of the command to send to the DM is lasts only 100 µs. We achieved a total latency of the loop of 1 ms, which is about 3 frames at 3.5 kHz. To reach this value, the DM was placed in a partial vacuum (∼100 Torr), to reduce the mechanical latency due to the resistance of the air pressure on the DM's membrane, which was about 300 µs. This latency is mostly limited by the transfer time of the image to the computer, which is about one frame. We are currently implementing a pixel streaming mode, where the calculation starts as soon as we receive portions of the image. This would actually accelerate the loop to ∼10 kHz, using partially updated images.

The PyWFS control loop has been validated on-sky, but is not yet fully optimal. We reached Strehl ratios of about 70% in H-band, with instantaneous measurements over 80%. These values are due to two effects:

1. A high spatial frequency noise in the PyWFS measurement, probably due to a sub-optimal Response Matrix (RM). The RM is taken on-sky, with the AO188 loop closed, and the PyWFS loop open. This RM is then taken in a regime where non-linearities can appear. A new approach is being implemented to take new RMs in a closed-loop scheme, to reduce any non-linearity.

2. Telescope vibrations are a main contributor of the Strehl degradation. These vibrations appear between 4 and 30 Hz, which should be low enough to be taken care of by the PyWFS, but they can have a very high

amplitude, up to 0.5 arcsec in the worst case, usually around the transit of the target. This amplitude puts the PyWFS as well as the DM in the nonlinear regime in tip/tilt, which degrades also all the other modes. Solutions are currently being implemented to reduce the vibrations at the source, to use the tip/tilt actuators of AO188 as a woofer, and to correct more efficiently the vibrations in the control loop by using predictive control.

3.2 On-Sky Demonstration Of Speckle Control

Even if the PyWFS delivers a stable wavefront, speckles around the PSF will still limit the detection of nearby objects. A way to cancel those speckles interferometrically is to use the method of speckle nulling, that detects the brightest speckles on one side of the image plane, then send a series of sine waves to the DM to find the best parameters to cancel them. By iterating this process, half of the speckle field is cleaned progressively.

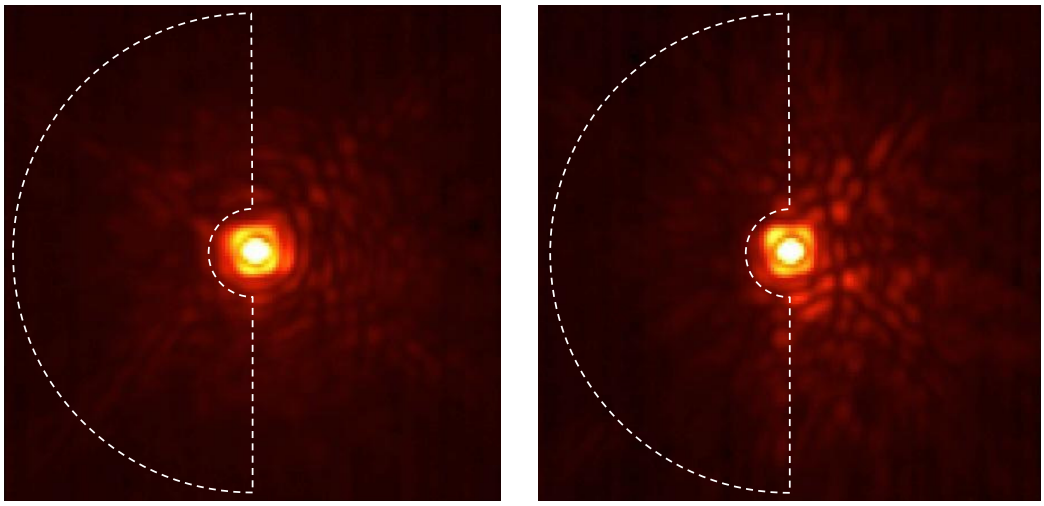

Figure 5. On-sky demonstration of speckle nulling on RX Boo, before (left) and after (right) correction. Both images are an average of 5000 50-µs integration images. The disk section is the control region, where the speckles become darker.

Originally, speckle nulling was implemented using the internal fast NIR camera, that can run at 170-Hz frame rate, but with 130 e^- readout noise. Figure 5 presents an example of validation on-sky on the target RX Boo, in H-band.[20] The left image is the PSF before correction, while the right image is after correction, in the white semi-disk. This validation was made without the PyWFS loop running, using only the correction provided by AO188. Even with a partial wavefront correction from the AO, we can still see a gain on the quasi-static speckles.

Speckle control is now being implemented using the SAPHIRA detector. SAPHIRA uses an array of HgCdTe avalanche photodiodes manufactured by SELEX that can run up to a few kHz, and has a sub-electron readout noise. Ultimately, speckle control is going to be performed using the MEC camera. the MKID detector inside the camera, besides having the same frame rate and readout noise as the SAPHIRA detector, can also provide the wavelength of the speckles. With the spectral information, it will be possible to compensate for the chromaticity of the atmosphere and reach an even higher contrast.

3.3 On-Sky Validation Of The Lyot-based Low-Order Wavefront Sensor

To achieve the best performance with SCExAO's small IWA coronagraphs, it is essential to correct for residual non-common path aberrations between the visible PyWFS and the NIR science channel. Refocusing the starlight rejected by the coronagraph in the Lyot plane, it is possible to measure the low-order aberrations. In this sensor, called Lyot-based Low-Order Wavefront Sensor (LLOWFS), each image of the camera is subtracted by a reference, and multiplied by a control matrix, obtained from a RM acquired beforehand.

Figure 6 presents an example of laboratory and on-sky validation of the LLOWFS, using a vector vortex coronagraph.[21] It was successfully tested in the laboratory with up to 35 corrected modes, using 4 different

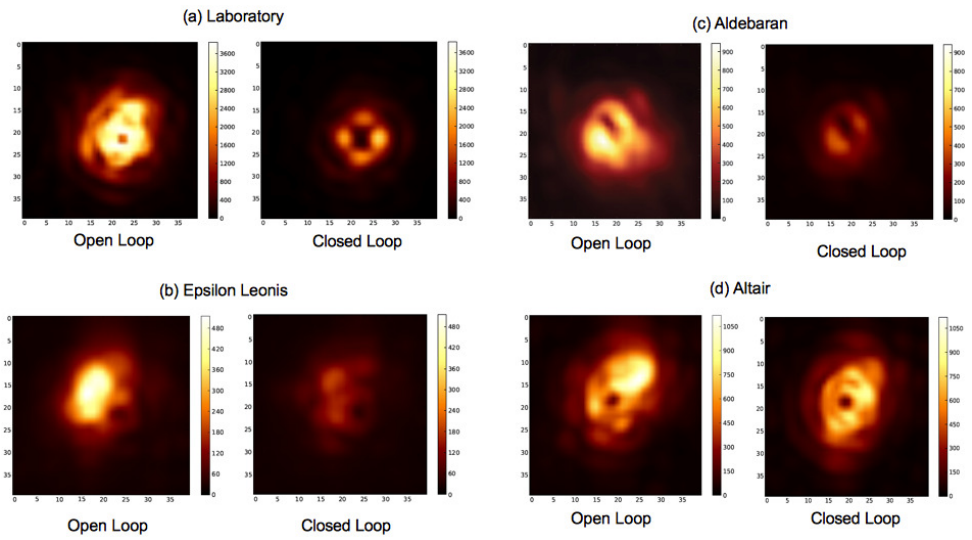

Figure 6. Laboratory and on-sky demonstration of Lyot-based Low Order Wavefront Sensor. Each image is the standard deviation of a sequence of 1000 images. We compare here open and closed-loop images, with the same intensity scale: a darker standard deviation indicates a more stable PSF.

coronagraphs: vector vortex, 4-quadrant phase mask (4QPM), 8OPM and PIAA coronagraph. On-sky, we demonstrated the correction of up to 15 Zernike modes.

3.4 First Demonstration Of A NIR PyWFS Using Roof Prisms

One of the key technologies essential for a high contrast imager on a 30-m class telescope is a NIR wavefront sensor. Usually, wavefront sensing is performed in the visible, due to the speed and quality of detectors in these wavelengths. But because the science is performed in the NIR, even with a perfect correction in the visible, the chromatic residual due to the chromaticity of the atmosphere will always limit the detection limit. Sensing the wavefront at wavelengths closer to the science bandwidth is key to reduce these chromatic effects.

With the development of efficient and fast NIR detectors like the SELEX of SAPHIRA, it is now possible to build a PyWFS in the H-band that can run at several kHz.

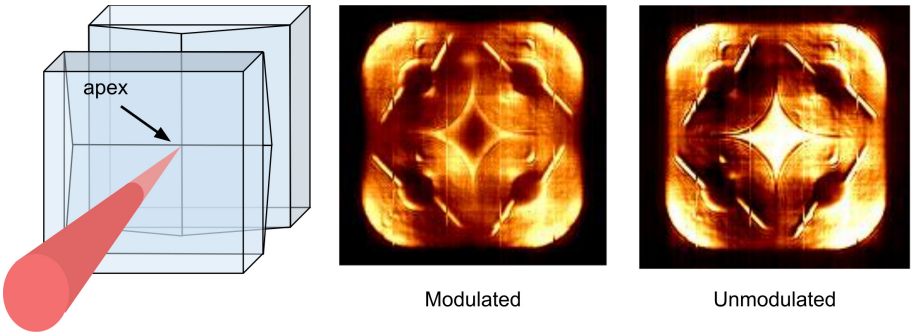

Figure 7. Laboratory demonstration of an H-band Pyramid Wavefront Sensor using two perpendicular roof prisms (left), in a modulated (middle) and unmodulated (right) configuration.

The second challenge for a PyWFS is the pyramid optics itself. Indeed, it is very challenging to have an optic with a good quality apex, where the 4 surfaces join exactly at the same point. To work around this problem, the solution presented in Fig. 7 is to use two roof prisms —much easier to manufacture—, and place them so that their ridges are orthogonal and almost touching each other. The beam is then focused in the middle of the two

prisms, as it would be on the apex of a regular pyramid. Figure 7 also presents a laboratory demonstration of such a pyramid in H-band, using the SAPHIRA detector. This simple design will allow for pyramid wavefront sensors to be more readily deployed for current and future instruments.

This type of roof prism pyramid was also designed to replace the pyramid optics currently used by the visible PyWFS, which has been done recently. It appears that this pyramid performs as well as the MagAO pyramid in visible wavelengths.

3.5 Preliminary Science Results

Since the ExAO loop is not yet fully commissioned, and most of SCExAO's modules rely on a good correction of the wavefront, the first science results presented in this paper are not optimal yet. But even with a 70% Strehl ratio, the images delivered by HiCIAO are about 3 times better, in IWA and Signal-to-Noise Ratio (SNR) than with AO188 alone.

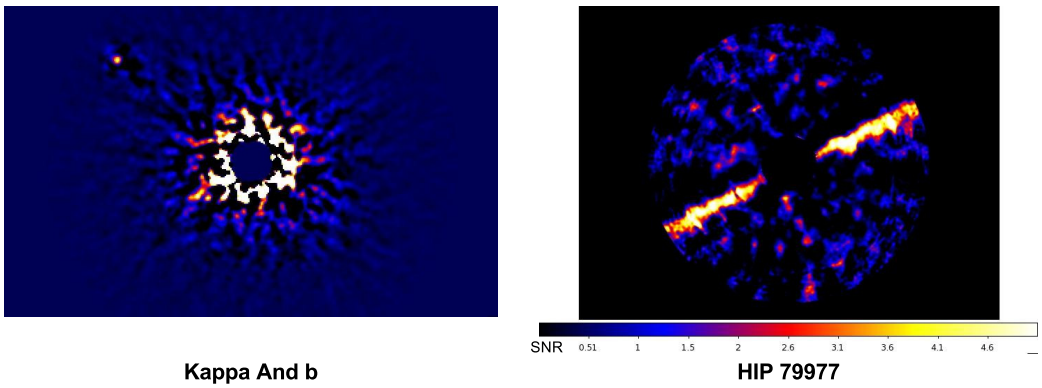

Figure 8. Preliminary science results with the extreme AO of SCExAO: the giant planet or brown dwarf κ And b (left), and the protoplanetary disk HIP 79977 (right). *Courtesy of Thayne Currie.*

Figure 8 (left) presents an image of the giant planet/brown dwarf κ Andromedae b, as a clear detection with a SNR $\sim$100, much better than the first discovery made by HiCIAO as part of the SEEDS survey. Figure 8 (right) is an image of the protoplanetary disk around HIP 79977, with a SNR between 3 and 7 (2 to 3 times better than HiCIAO alone), and a detection closer to the star at about 300 mas (3 times closer than HiCIAO).

4. FROM SUBARU TO TMT

4.1 More Exciting Science

Simulations shows that it is impossible to image any rocky planet in the habitable zone of nearby stars with a 8-m class telescope. A sufficient contrast cannot be achieved, and the resolution of the telescope is just not good enough. But by increasing the telescope size to 30 m, new science can be reached. Figure 9 presents the contrast and angular separation of rocky planets in the HZ of the nearest stars —supposing that each star has one. the color of each circle indicates the stellar type, while its size indicates the distance to our Sun.

A SCExAO-like instrument on a telescope like TMT would be able to reach 10^{-8} contrast at $\sim$1 λ/D, and therefore would be able to detect and characterize spectrally Earth-like planets in the HZ of about 50 nearby stars —mostly M-type stars. In this case, the low hanging fruit would be a planet around Proxima Centauri, requiring a contrast of "only" a few 10^{-7}. The technologies demonstrated on SCExAO are key to accessing the contrasts required for imaging reflected light, habitable zone planets.

The goal of SCExAO is to demonstrate and validate performances on Subaru prior to deployment on TMT. The system would then be ready to go as first light visitor instrument, with well understood science performance. It would then mitigate risks and minimize need for engineering and commissioning time on TMT. Finally, it would benefit from years of practice and experience on Subaru (loop control, data reduction algorithms, observing

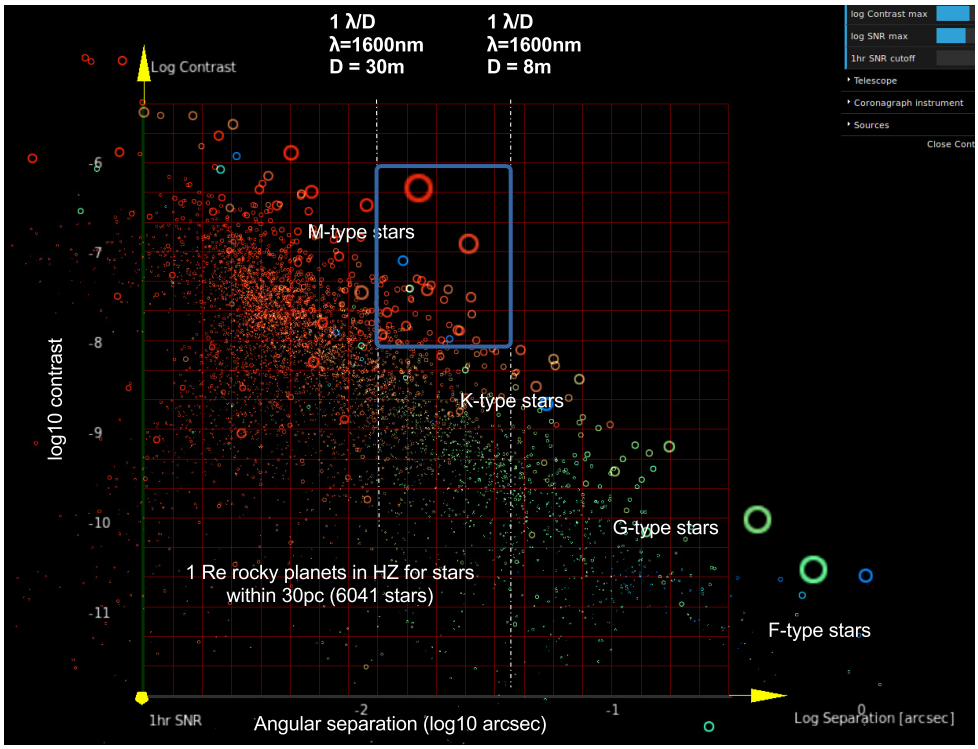

Figure 9. Science case for a SCExAO-like instrument on TMT. This figure shows the contrast and angular separation for Earth-like planets in the HZ of the closest stars. Around about 50 M-type stars, rocky planets in the HZ (if any) could be imaged and their spectra acquired, assuming a 10^{-8} contrast limit and 1 λ/D IWA.

strategy). Its results would be beneficial for a second generation, more capable ExAO system that would be developed at the same time.

4.2 PIAACMC: A Coronagraph For The Complex Pupil Of TMT

The three ELTs currently in development have all pretty complex pupils. Segments, central obstructions and spiders are a challenge to design efficient coronagraphs. One method combines the lossless apodization of the PIAA and the complexity of phase mask coronagraphs: the PIAACMC.[22] As shown in Fig. 10, the beam is slightly apodized by two aspherical surfaces, and focused on a focal plane phase mask. This mask is composed of

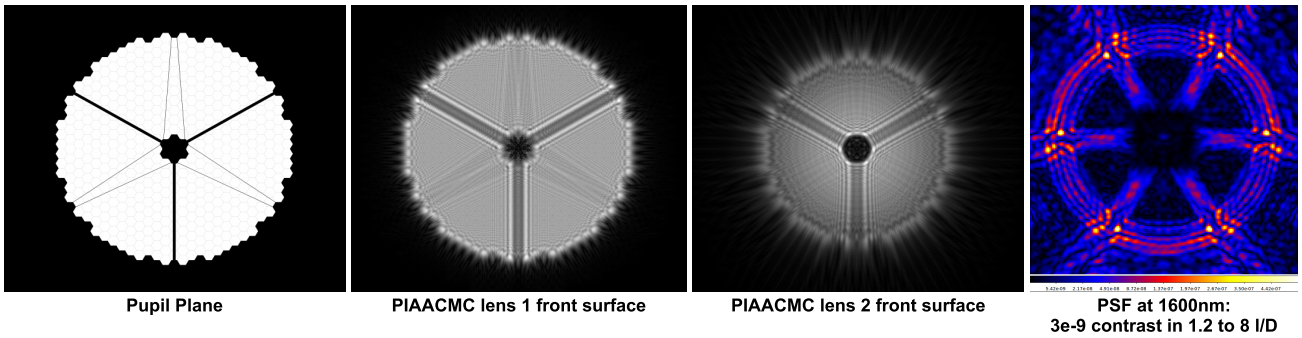

Figure 10. Effect of the PIAACMC's optics on the beam, from the TMT pupil (left), to the two PIAACMC apodizing lenses (middle), to the final focal plane, after the complex phase mask and the Lyot stop (right). The contrast reached by such a coronagraph is 3×10^{-9} between 1.2 and 8 λ/D.

hundreds of segments much smaller than λ/D, and designed so the light is rejected outside of the pupil over the largest bandwidth possible. This type of coronagraph can achieve very high contrasts at 1 λ/D, necessary for the detection of rocky planets. Such a coronagraph will very soon be implemented on SCExAO, characterized and tested in the laboratory and on-sky.

4.3 A PyWFS And Speckle Control To Reach The Highest Contrast On TMT

As we can see with the example of the PIAACMC, coronagraphs can now reach 1–2 λ/D IWA at $\sim 10^{-7}$ raw contrast in NIR on almost any pupil this is several orders of magnitude better than today's best ExAO systems. The challenge is now fundamentally on the wavefront control and the calibration.

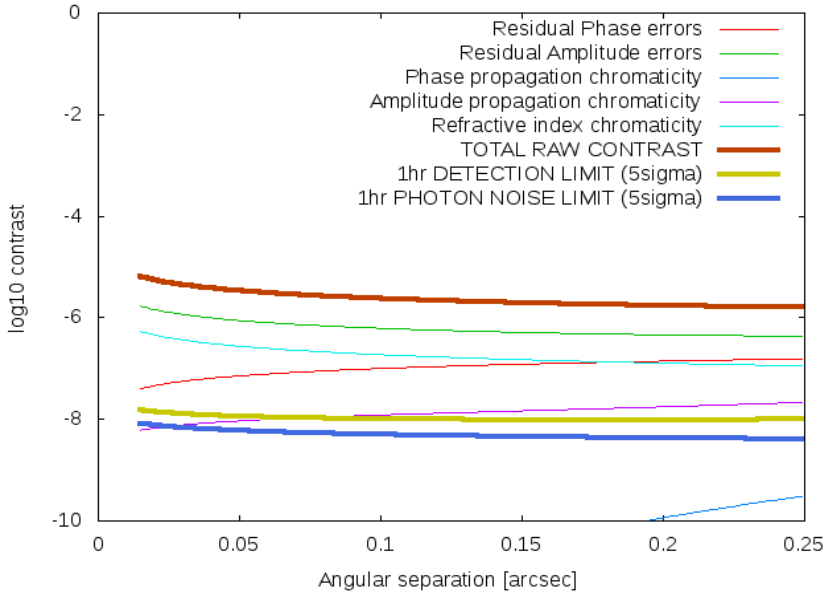

Figure 11. Contrast limits at different angular separations, for the raw contrast and the detection limit after post-processing.

The simulation presented in Fig. 11 simulates a high-contrast imager equipped with a visible PyWFS, a NIR speckle control and a PIAACMC coronagraph on a 30-m telescope. The visible PyWFS is running at 10 kHz and the NIR speckle control at 1 kHz. The final raw contrast is mostly limited by residual amplitude and phase errors, as well as the chromaticity of the refractive index of the air layer. Even with the best wavefront correction, only a raw contrast of 10^{-6} can be achieved. The only way to go deeper in contrast is to calibrate the residual speckles in post-processing, using enough exposures on-sky. The detection limit can then go down to 10^{-8}, close to the photon noise limit.

4.4 Coherent Differential Imaging

An innovative way to cancel speckles in post-processing is to use all the coherence information coming from the speckle control. Indeed, when the speckle field is probed for speckle control, only the starlight interfere with itself, the planet light is untouched. So even if the speckles are not corrected by the DM, the coherence of the light in the speckle field can still be extracted.

Figure 12 presents an example of coherent differential imaging. The two symmetric regions —the gray rectangles— around the PSF on the top left of the figure are probed using the DM. With 4 different probes and the unprobed image, it is possible to decompose the light in those regions (right part of the figure). The total light is then the sum of a complex coherent part coming from speckles and diffraction, and incoherent part, coming from the object we want to study. It is then possible to detect a planet even if the speckle field is one or two orders of magnitude brighter.

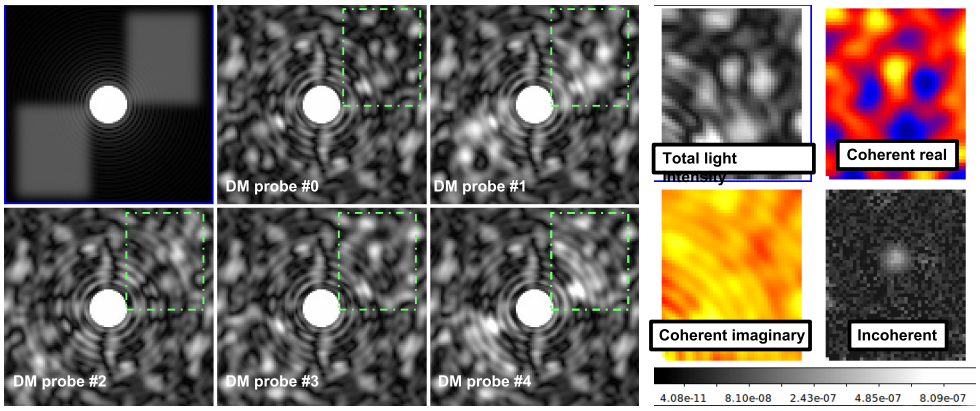

Figure 12. Principle of coherent differential imaging: A set of probes is sent to the DM (left), and with the resulting images, the speckle field is decomposed into complex coherent light and incoherent light (right).

5. CONCLUSION

SCExAO is a unique instrument that will soon be one of the most powerful high-contrast imagers. Its main advantage is its modularity, its capacity to test new technologies necessary for the next generation instruments. Once all its modules are commissioned, SCExAO will be close to the optimal design for high-contrast imagers for ELTs. Since none of the three ELTs is planning a high-contrast imager as a first generation instrument, we would have to wait until at least 2035 before one becomes available. As a visitor instrument on TMT, SCExAO would have the best opportunity to access a unique science case, and test different technologies for more advanced instruments.

REFERENCES

[1] Jovanovic, N., Martinache, F., Guyon, O., Clergeon, C., Singh, G., Kudo, T., Garrel, V., Newman, K., Doughty, D., Lozi, J., Males, J., Minowa, Y., Hayano, Y., Takato, N., Morino, J., Kuhn, J., Serabyn, E., Norris, B., Tuthill, P., Schworer, G., Stewart, P., Close, L., Huby, E., Perrin, G., Lacour, S., Gauchet, L., Vievard, S., Murakami, N., Oshiyama, F., Baba, N., Matsuo, T., Nishikawa, J., Tamura, M., Lai, O., Marchis, F., Duchene, G., Kotani, T., and Woillez, J., "The Subaru Coronagraphic Extreme Adaptive Optics System: Enabling High-Contrast Imaging on Solar-System Scales," *Pub. Astron. Soc. Pacific* **127**, 890–910 (Oct. 2015).

[2] Minowa, Y., Hayano, Y., Oya, S., Watanabe, M., Hattori, M., Guyon, O., Egner, S., Saito, Y., Ito, M., Takami, H., Garrel, V., Colley, S., Golota, T., and Iye, M., "Performance of Subaru adaptive optics system AO188," in [*Adaptive Optics Systems II*], *Proc. Soc. Photo-Opt. Instrum. Eng.* **7736**, 77363N (July 2010).

[3] Macintosh, B., Graham, J. R., Ingraham, P., Konopacky, Q., Marois, C., Perrin, M., Poyneer, L., Bauman, B., Barman, T., Burrows, A. S., Cardwell, A., Chilcote, J., De Rosa, R. J., Dillon, D., Doyon, R., Dunn, J., Erikson, D., Fitzgerald, M. P., Gavel, D., Goodsell, S., Hartung, M., Hibon, P., Kalas, P., Larkin, J., Maire, J., Marchis, F., Marley, M. S., McBride, J., Millar-Blanchaer, M., Morzinski, K., Norton, A., Oppenheimer, B. R., Palmer, D., Patience, J., Pueyo, L., Rantakyro, F., Sadakuni, N., Saddlemyer, L., Savransky, D., Serio, A., Soummer, R., Sivaramakrishnan, A., Song, I., Thomas, S., Wallace, J. K., Wiktorowicz, S., and Wolff, S., "First light of the Gemini Planet Imager," *Proceedings of the National Academy of Science* **111**, 12661–12666 (Sept. 2014).

[4] Beuzit, J.-L., Feldt, M., Dohlen, K., Mouillet, D., Puget, P., Wildi, F., Abe, L., Antichi, J., Baruffolo, A., Baudoz, P., Boccaletti, A., Carbillet, M., Charton, J., Claudi, R., Downing, M., Fabron, C., Feautrier, P., Fedrigo, E., Fusco, T., Gach, J.-L., Gratton, R., Henning, T., Hubin, N., Joos, F., Kasper, M., Langlois, M., Lenzen, R., Moutou, C., Pavlov, A., Petit, C., Pragt, J., Rabou, P., Rigal, F., Roelfsema, R., Rousset, G., Saisse, M., Schmid, H.-M., Stadler, E., Thalmann, C., Turatto, M., Udry, S., Vakili, F., and Waters, R., "SPHERE: a 'Planet Finder' instrument for the VLT," in [*Ground-based and Airborne Instrumentation for Astronomy II*], *Proc. Soc. Photo-Opt. Instrum. Eng.* **7014**, 701418 (July 2008).

[5] Sanders, G. H., "The Thirty Meter Telescope (TMT): An International Observatory," *Journal of Astrophysics and Astronomy* **34**, 81–86 (June 2013).

[6] McElwain, M. W., Brandt, T. D., Janson, M., Knapp, G. R., Peters, M. A., Burrows, A. S., Carlotti, A., Carr, M. A., Groff, T., Gunn, J. E., Guyon, O., Hayashi, M., Kasdin, N. J., Kuzuhara, M., Lupton, R. H., Martinache, F., Spiegel, D., Takato, N., Tamura, M., Turner, E. L., and Vanderbei, R. J., "Scientific design of a high contrast integral field spectrograph for the Subaru Telescope," in [*Ground-based and Airborne Instrumentation for Astronomy IV*], *Proc. Soc. Photo-Opt. Instrum. Eng.* **8446**, 84469C (Sept. 2012).

[7] Mazin, B. A., Bumble, B., Meeker, S. R., O'Brien, K., McHugh, S., and Langman, E., "A superconducting focal plane array for ultraviolet, optical, and near-infrared astrophysics," *Opt. Express* **20**, 1503 (Jan. 2012).

[8] Esposito, S. and Riccardi, A., "Pyramid Wavefront Sensor behavior in partial correction Adaptive Optic systems," *Astron. Astrophys.* **369**, L9–L12 (Apr. 2001).

[9] Bordé, P. J. and Traub, W. A., "High-Contrast Imaging from Space: Speckle Nulling in a Low-Aberration Regime," *Astrophys. J.* **638**, 488–498 (Feb. 2006).

[10] Mawet, D., Serabyn, E., Liewer, K., Hanot, C., McEldowney, S., Shemo, D., and O'Brien, N., "Optical Vectorial Vortex Coronagraphs using Liquid Crystal Polymers: theory, manufacturing and laboratory demonstration," *Opt. Express* **17**, 1902–1918 (Feb. 2009).

[11] Murakami, N., Nishikawa, J., Yokochi, K., Tamura, M., Baba, N., and Abe, L., "Achromatic Eight-octant Phase-mask Coronagraph using Photonic Crystal," *Astrophys. J.* **714**, 772–777 (May 2010).

[12] Guyon, O., "Phase-induced amplitude apodization of telescope pupils for extrasolar terrestrial planet imaging," *Astron. Astrophys.* **404**, 379–387 (June 2003).

[13] Singh, G., Martinache, F., Baudoz, P., Guyon, O., Matsuo, T., Jovanovic, N., and Clergeon, C., "Lyot-based Low Order Wavefront Sensor for Phase-mask Coronagraphs: Principle, Simulations and Laboratory Experiments," *Pub. Astron. Soc. Pacific* **126**, 586–594 (June 2014).

[14] Lozi, J., Martinache, F., and Guyon, O., "Phase-Induced Amplitude Apodization on Centrally Obscured Pupils: Design and First Laboratory Demonstration for the Subaru Telescope Pupil," *Pub. Astron. Soc. Pacific* **121**, 1232–1244 (Nov. 2009).

[15] Jovanovic, N., Guyon, O., Martinache, F., Schwab, C., and Cvetojevic, N., "How to inject light efficiently into single-mode fibers," in [*Ground-based and Airborne Instrumentation for Astronomy V*], *Proc. Soc. Photo-Opt. Instrum. Eng.* **9147**, 91477P (July 2014).

[16] Atkinson, D., Hall, D., Baranec, C., Baker, I., Jacobson, S., and Riddle, R., "Observatory deployment and characterization of SAPHIRA HgCdTe APD arrays," in [*High Energy, Optical, and Infrared Detectors for Astronomy VI*], *Proc. Soc. Photo-Opt. Instrum. Eng.* **9154**, 915419 (July 2014).

[17] Norris, B. R. M., Tuthill, P. G., Ireland, M. J., Lacour, S., Zijlstra, A. A., Lykou, F., Evans, T. M., Stewart, P., Bedding, T. R., Guyon, O., and Martinache, F., "Probing dusty circumstellar environments with polarimetric aperture-masking interferometry," in [*Optical and Infrared Interferometry III*], *Proc. Soc. Photo-Opt. Instrum. Eng.* **8445**, 844503 (July 2012).

[18] Huby, E., Perrin, G., Marchis, F., Lacour, S., Kotani, T., Duchêne, G., Choquet, E., Gates, E. L., Woillez, J. M., Lai, O., Fédou, P., Collin, C., Chapron, F., Arslanyan, V., and Burns, K. J., "FIRST, a fibered aperture masking instrument. I. First on-sky test results," *Astron. Astrophys.* **541**, A55 (May 2012).

[19] Close, L. M., Males, J. R., Morzinski, K., Kopon, D., Follette, K., Rodigas, T. J., Hinz, P., Wu, Y.-L., Puglisi, A., Esposito, S., Riccardi, A., Pinna, E., Xompero, M., Briguglio, R., Uomoto, A., and Hare, T., "Diffraction-limited Visible Light Images of Orion Trapezium Cluster with the Magellan Adaptive Secondary Adaptive Optics System (MagAO)," *Astrophys. J.* **774**, 94 (Sept. 2013).

[20] Martinache, F., Guyon, O., Jovanovic, N., Clergeon, C., Singh, G., Kudo, T., Currie, T., Thalmann, C., McElwain, M., and Tamura, M., "On-Sky Speckle Nulling Demonstration at Small Angular Separation with SCExAO," *Pub. Astron. Soc. Pacific* **126**, 565–572 (June 2014).

[21] Singh, G., Lozi, J., Guyon, O., Baudoz, P., Jovanovic, N., Martinache, F., Kudo, T., Serabyn, E., and Kuhn, J., "On-Sky Demonstration of Low-Order Wavefront Sensing and Control with Focal Plane Phase Mask Coronagraphs," *Pub. Astron. Soc. Pacific* **127**, 857–869 (Oct. 2015).

[22] Guyon, O., Martinache, F., Belikov, R., and Soummer, R., "High Performance PIAA Coronagraphy with Complex Amplitude Focal Plane Masks," **190**, 220–232 (Oct. 2010).